Solar modulation of GCR electrons over the 23rd solar minimum with PAMELA

2015 J. Phys.: Conf. Ser. 632 012073

(http://iopscience.iop.org/1742-6596/632/1/012073)

Journal of Physics: Conference Series **632** (2015) 012073 doi:10.1088/1742-6596/632/1/012073

Solar modulation of GCR electrons over the 23rd solar minimum with PAMELA

R. Munini[1,2], V. Di Felice[3], O. Adriani[4,5], G. C. Barbarino[6,7], G. A. Bazilevskaya[8],R. Bellotti[9,10], M. Boezio[2], E. A. Bogomolov[11], M. Bongi[4,5], V. Bonvicini[2], S. Bottai[5], A. Bruno[9,10], F. Cafagna[10], D. Campana[7], P. Carlson[12], M. Casolino[3,14], G. Castellini[15], C. De Donato[3], C. De Santis[13], N. De Simone[3], V. Formato[1,2], A. M. Galper[16], A. V. Karelin[16], S. V. Koldashov[16], S. Koldobskiy[16], S. Y. Krutkov[11], A. N. Kvashnin[8], A. Leonov[16],V. Malakhov[16], L. Marcelli[13], M. Martucci[13,17], A. G. Mayorov[16], W. Menn[18], M Merge'[3,13], V. V. Mikhailov[16],E. Mocchiutti[2], A. Monaco[9,10], N. Mori[5], G. Osteria[7], F. Palma[3,13], B. Panico[7] P. Papini[5], M. Pearce[12], P. Picozza[3,13], M. Ricci[17], S. B. Ricciarini[15], R. Sarkar[2], V. Scotti[6,7], M. Simon[18], R. Sparvoli[3,13], P. Spillantini[4,5], Y. I. Stozhkov[8], A. Vacchi[2], E. Vannuccini[5], G. Vasilyev[11], S. A. Voronov[16], Y. T. Yurkin[16], G. Zampa[2], N. Zampa[2], M. S. Potgieter [21], E.E. Vos [21].

[1]University of Trieste, Department of Physics, I-34147 Trieste, Italy
[2]INFN, Sezione di Trieste, I-34149 Trieste, Italy
[3]INFN, Sezione di Rome "Tor Vergata", I-00133 Rome, Italy
[4]University of Florence, Department of Physics, I-50019 Sesto Fiorentino, Florence, Italy
[5]INFN, Sezione di Florence, I-50019 Sesto Fiorentino, Florence, Italy
[6]University of Naples "Federico II", Department of Physics, I-80126 Naples, Italy
[7]INFN, Sezione di Naples, I-80126 Naples, Italy
[8]Lebedev Physical Institute, RU-119991, Moscow, Russia
[9]University of Bari, Department of Physics, I-70126 Bari, Italy
[10]INFN, Sezione di Bari, I-70126 Bari, Italy
[11]Ioffe Physical Technical Institute, RU-194021 St. Petersburg, Russia
[12]KTH, Department of Physics, and the Oskar Klein Centre for Cosmoparticle Physics, AlbaNova University Centre, SE-10691 Stockholm, Sweden
[13]University of Rome "Tor Vergata", Department of Physics, I-00133 Rome, Italy
[14]RIKEN, Advanced Science Institute, Wako-shi, Saitama, Japan
[15]IFAC, I-50019 Sesto Fiorentino, Florence, Italy
[16]National Research Nuclear University MEPhI, RU-115409 Moscow
[17]INFN, Laboratori Nazionali di Frascati, Via Enrico Fermi 40, I-00044 Frascati, Italy
[18]Universität Siegen, Department of Physics, D-57068 Siegen, Germany
[19]INFN, Sezione di Perugia, I-06123 Perugia, Italy
[20]Agenzia Spaziale Italiana (ASI) Science Data Center, I-00044 Frascati, Italy
[21]North-West University, Centre for Space Research,2520 Potchefstroom, South Africa

E-mail: Riccardo.Munini@ts.infn.it

Abstract. The satellite-borne PAMELA experiment has been continuously collecting data since 15th June 2006, when it was launched from the Baikonur cosmodrome to detect the charged component of cosmic rays over a wide energy range and with unprecedented statistics. The apparatus design is particularly suited for particle and antiparticle identification. The PAMELA experiment has measured the electron spectrum at Earth in great detail, extending up to about 100 GeV and down to about 200 MeV. The galactic cosmic ray electron spectra for 2007 and 2009, i.e. measured during the A<0 solar minimum of solar cycle 23, are presented. These fluxes provide important information for the study of charge dependent solar modulation effects.

1. Introduction

The study of the precise measurements of the energy spectrum of cosmic ray electrons provide fundamental information regarding their origin and propagation. However the majority of the measurements where obtained with experiments well inside the heliosphere. Therefore the effects of the propagation and modulation of galactic cosmic rays in the heliosphere cannot be neglected. As cosmic rays traverse the turbulent magnetic field embedded into the solar wind particles are scattered by its irregularities and undergo convection and adiabatic deceleration in the expanding solar wind. Gradient and curvature drifts have also an effect, that is dominant during periods of minimum solar activity. Cosmic rays with rigidities up to tens of GV are affected but the largest effect is seen at low rigidities (less than a few GV). Furthermore, drift models predict a clear charge-sign dependence for the modulation of cosmic rays [1], whose effects are expected to be particularly evident at energies below a few GeV. During so-called A [1] < 0 polarity cycles like solar cycle 23, when the heliospheric magnetic field is directed toward the Sun in the northern hemisphere, negatively-charged particles will drift inward primarily through the polar regions of the heliosphere. Conversely, positively-charged particles will drift inward primarily through the equatorial regions of the heliosphere, encountering the wavy heliospheric current sheet in the process. The situation reverses when the solar magnetic field changes its polarity at each solar maximum. This was shown by the electron ($e^- + e^+$) and proton measurements from few up to several hundreds MeV by the KET instrument on board the Ulysses spacecraft [2] that explored the high latitude regions of the inner heliosphere from 1990 to 2009. Similar conclusion can be drawn by the electron ($e^- + e^+$) data collected by the balloon-born experiment LEE over several decades [3].

The most recent period of solar minimum activity and the consequent minimum modulation conditions for cosmic rays were unusual. It was expected that the new activity cycle would begin early in 2008. Instead solar minimum modulation conditions continued until the end of 2009 when the largest fluxes of galactic cosmic rays since the beginning of the space age were recorded [4]. This period of prolonged solar minimum activity is well suited to study the modulation processes that affect the propagation of galactic cosmic rays inside the heliosphere.

PAMELA (Payload for Antimatter Matter Exploration and Light-nuclei Astrophysics) is a satellite-borne experiment designed to make long duration measurements of the cosmic radiation [5]. Results on the effects of the solar modulation on the energy spectra of galactic cosmic-ray protons in the period July 2006-December 2009 have already been published [6] by the PAMELA collaboration. Here we present new results on the long-term variation in the energy spectrum of galactic cosmic-ray electrons (e^-) measured down to 200 MeV and with no atmospheric overburden. This set of measurements allows detailed analysis of the propagation of cosmic rays in the heliosphere and the study of particle drift effects to be performed.

[1] In the complex sun magnetic field the dipole term nearly always dominates the magnetic field of the solar wind. A is defined as the projection of this dipole on the solar rotation axis.

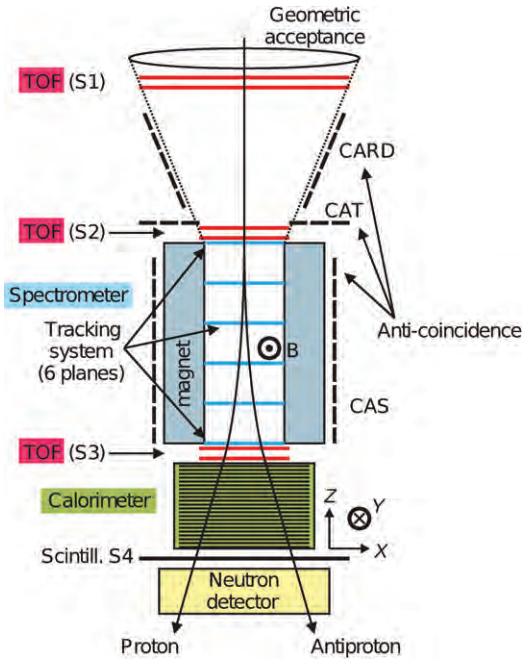

Figure 1. PAMELA and its sub-detectors.

2. The PAMELA instrument

The PAMELA experiment was launched on June 15^{th} 2006 from the Bajkonur cosmodrome on-board of the Resurs DK1 satellite and, since then, it has been almost continuously taking data. The instrument is following a high inclination (70°) orbit, ideal condition to observe the solar modulation of galactic cosmic rays down to very low energies (< 100 MeV).

The PAMELA spectrometer [5] was designed and built to study the antimatter component of cosmic rays from tens of MeV up to hundreds of GeV and with a significant increase in statistics with respect to previous experiments. To reach this goal the apparatus was optimized for the study of Z = 1 particles and to reach a high level of electron-proton discrimination.

The apparatus comprises the following subdetectors, arranged as shown schematically in Figure 1 (from top to bottom): a time-of-flight system (TOF S1, S2, S3); a magnetic spectrometer; an anticoincidence system (CARD, CAT, CAS); an electromagnetic imaging calorimeter; a shower tail catcher scintillator (S4) and a neutron detector.

The central components of PAMELA are a permanent magnet and a tracking system composed of six planes of double-sided silicon sensors, which form the magnetic spectrometer. The main task of the magnetic spectrometer is to measure the particle rigidity $\rho = \mathrm{pc/Ze}$ (p and Ze being respectively the particle momentum and charge, and c the speed of light) and the ionization energy losses (dE/dx). The rigidity measurement is done through the reconstruction of the trajectory based on the impact points on the tracking planes and the resulting determination of the curvature due to the Lorentz force. The Time-of-Flight (ToF) system comprises three double layers of plastic scintillator paddles with the first two placed above and the third immediately below the magnetic spectrometer. The ToF system provides the measurements of the particle velocity combining the time of passage information with the track length derived from the magnetic spectrometer. By measuring the particle velocity, direction and curvature the spectrometer can distinguish between downgoing particles and upgoing splash [2] albedo particles and separate negatively from positively-charged particles.

[2] Upgoing secondary particles resulting from the interaction of high energy CRs with the atmosphere.

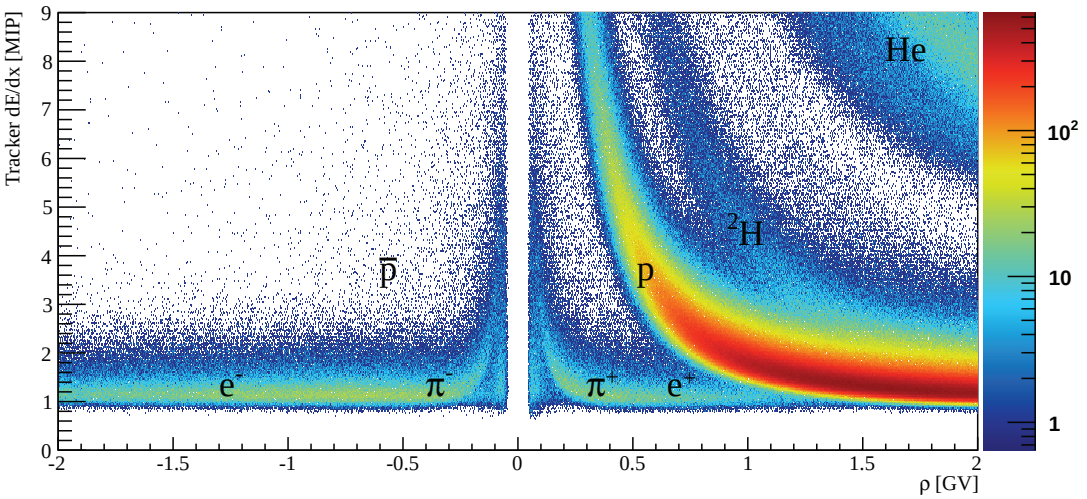

Figure 2. Rigidity distribution for the mean energy release on the tracker planes expressed in minimum ionizing particle units, MIP. On the positive side protons dominate. Below 300 MV is clearly visible the secondary pion contamination.

The sampling imaging calorimeter (16.3 radiation lengths, 0.6 interaction lengths) is used for hadron-lepton separation, using topological and energetic informations about the shower development in the calorimeter. The shower tail catcher and the neutron detector beneath provide additional information for the discrimination. An anticoincidence system is used to reject spurious events in the off-line phase.

The total weight of PAMELA is 470 kg while the power consumption is 355 W. A more detailed description of the instruments and the data handling can be found in [5].

3. Data analysis

A first selection on the goodness of the reconstructed track, expressed in terms of the χ^2 of the fit, was made in order to obtain a sample of events with a reliable reconstructed rigidity. Only single track events were selected and a minimum of three impact points on the non bending view and four impact points on the bending view in the tracking system were required. Furthermore to increase the spectrometer performance the track was required to be reconstructed inside a fiducial volume bounded 0.15 cm from the magnet cavity walls. Downward going particles were selected requiring that their velocities, $\beta = v/c$, measured by the ToF system were greater than zero, hence rejecting splash albedo particles.

Figure 2 illustrates the rigidity distribution for the mean ionization losses in the tracker planes for events selected as described above. On the positive side the protons signal dominates. For the identification of the electrons three sources of contamination were studied:

- Anti-protons: the galactic anti-proton component represents a contamination of a few percent over the entire rigidity range.
- Pions: this secondary component is locally produced by cosmic rays interacting with the PAMELA structure or pressure vessel. This component had already been studied for the anti-proton analysis [7]. Pion contamination reaches a maximum value around 200-300 MV amounting to a few percent of the electrons signal and decrease rapidly becoming negligible, according to simulation, above 1 GV. This component is clearly visible below 300 MV in figure 2 both for positive and negative rigidities.

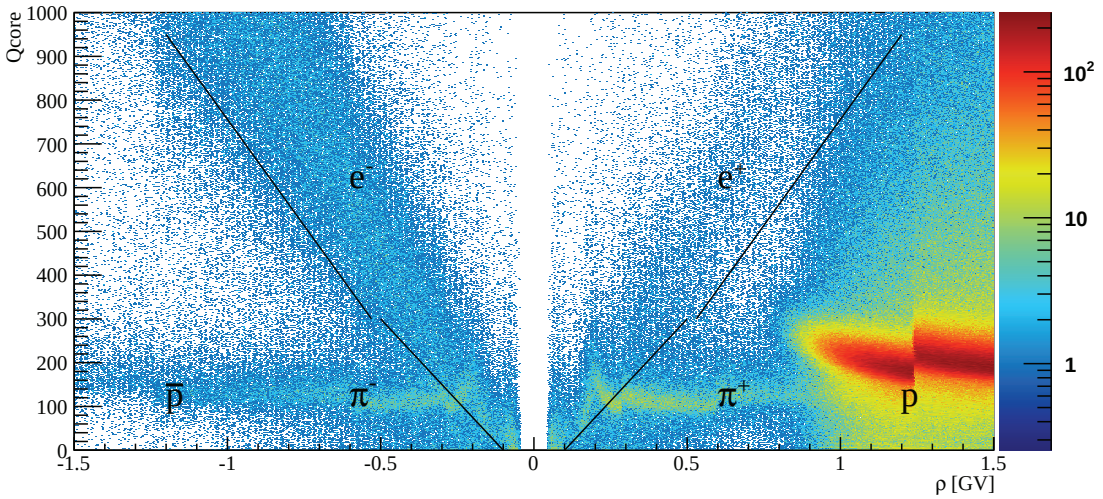

Figure 3. Qcore rigidity distribution. On the positive side above 1 GV the proton component dominates. Pions are present on both sides and overlap with electrons and positrons below 300 MV. This residual contamination was removed using selections on other calorimeter variables. The black lines represent the electron selection on Qcore.

- Spillover protons: this contamination consists of high energy ($>$ 10 GV) protons reconstructed as low energy ($<$ 1 GV) negatively-charged particles. Because of the presence of spurious hits in the tracker planes, a wrong sign of the curvature is assigned to the reconstructed tracks of these events. These events are significant at energies below 1 GeV and amount to a few percent of the electrons signal.

Requiring $\beta > 0.9$, tracker dE/dx $<$ 1.8 MIP and ToF dE/dx$<$ 3 MIP, anti-protons and pions were rejected up to 1 GeV and 250 MeV respectively. Below 1 GeV the negatively charged events remaining after the velocity and dE/dx selections were predominately electrons with a small residual pion contamination. The majority of the pion events had hits in the top anticoincidence scintillators, therefore they were removed requiring no activity on CARD and CAT. Being relativistic, spillover protons were unaffected by these selections.

The residual pion and proton contaminations were removed using the calorimeter informations. The calorimeter selections were developed using a Monte Carlo simulation of the PAMELA apparatus based on the GEANT4 code [8]. The simulation reproduces the entire PAMELA apparatus, including the pressure vessel, and was validated using particle beam data. The longitudinal and transverse segmentation of the calorimeter allow leptonic showers to be selected with high efficiency and small contamination above 300 MeV. The calorimeter electron selection was based on variables that emphasizes the differences between the leptonic and hadronic shower like the multiplication with increasing calorimeter depth and the collimation of the electromagnetic cascade along the track.

Figure 3 shows the distribution of one of these variables, Qcore, for the events passing the ToF, tracking and anticoincidence selections. This quantity, related to the multiplication of the leptonic shower, turned out to have large values for leptons, lower for non interacting and late interacting hadrons because of the limited longitudinal and transverse dispersion of the hadronic shower. The black line on figure 3 indicates the lower limit for electron selection based on this quantity. Combining several of these variables anti-proton and pion contamination were reduced to a negligible amount up to tens of GV [9].

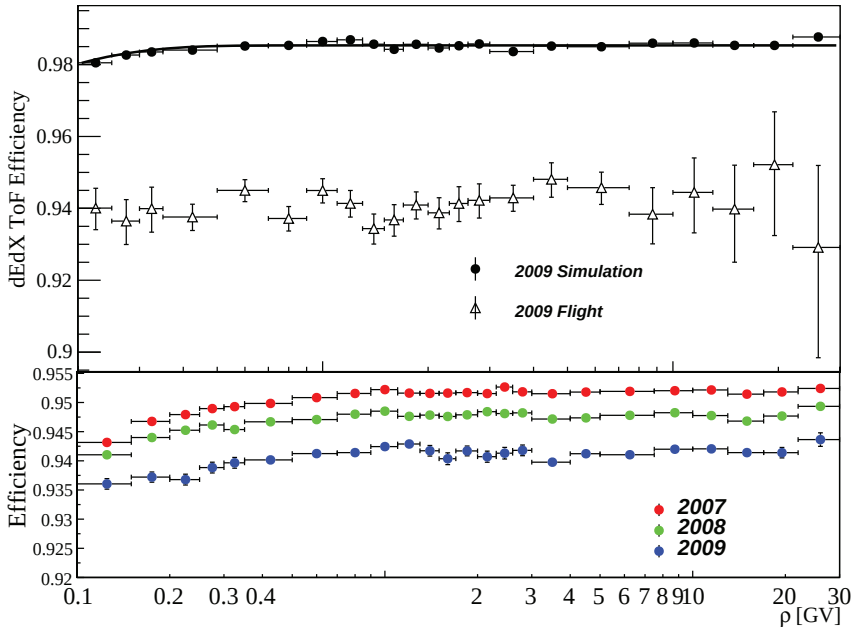

Figure 4. Top panel: comparison between the simulated and flight data ToF ionization losses efficiency. Black line represent a fit to the simulated data. Bottom panel: temporal evolution of the ToF ionization losses efficiency from 2007 to 2009.

The spillover protons were rejected using calorimeter variables that exploited the energy deposit in the last planes of the calorimeter. Electromagnetic showers below 1 GeV usually develop in the first half of the calorimeter instead of high energy protons that traverse the entire volume. A cut on the number of strips hit in the last 6 calorimeter planes rejected spillover protons without affecting significantly the electron signal.

After all these selections, the residual contamination of pions, anti-protons and spillover protons was estimated to be negligible over the entire energy range.

4. Results

The fluxes $\phi(\rho)$ are evaluated as follows:

$$\phi(\rho) = \frac{1}{\epsilon(\rho) \times G \times T \times \Delta\rho} \times N \tag{1}$$

where N is the number of selected events, $\epsilon(\rho)$ the overall selections efficiency, G the geometrical factor, T the live-time and $\Delta\rho$ the width of the rigidity bin.

The various efficiencies were estimated using both simulated and flight data. Tracker efficiency was obtained entirely from simulation. The anticoincidence and ToF ionization losses efficiencies were evaluated with simulation using the real data both as cross-check and to evaluate possible normalization factors. Figure 4 shows the efficiencies for the ToF ionization losses as a function of rigidity. The upper panel displays the comparison between the 2009 simulated and flight data. As can be seen from Figure 4 a constant normalization factor ($\sim 4\%$) is needed in order to match the two sets of data. It should be noted that the shape of the flight data is well reproduced by simulation. The black line is a fit to the simulated data. The efficiencies of the β and calorimeter selections were entirely evaluated using flight data.

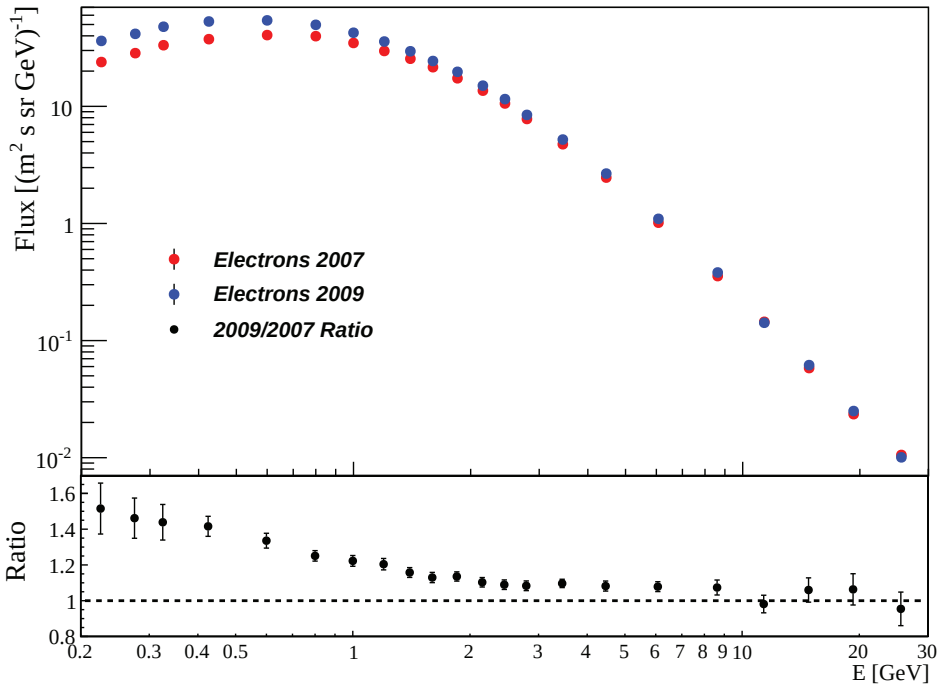

Figure 5. Top panel: 2007 and 2009 electron energy spectra as measured by PAMELA. Bottom panel: ratio between the 2009 and 2007 electron fluxes. The solar modulation is clearly visible and became negligible above $\sim$ 20 GeV. The error bars indicate only statistical uncertainties.

The temporal dependence of the efficiencies was carefully studied. As an example the lower panel of figure 4 show the dEdX ToF efficiencies for three different time period. A small dependence on time is present due to vary calibrations of the read-out signals over the years. The tracker efficiency was estimated using the simulation and it was found to decrease with time due to a progressive deterioration of the read-out chips [6].

The live time was provided by an on-board clock that timed the periods during which the apparatus is waiting for a trigger. The geometrical factor was estimated with simulation to be constant at 19.9 cm^2 sr in the energy range of interest.

Electron rigidity spectra were obtained for different intervals of vertical geomagnetic cutoff rigidities, estimated in the Störmer approximation [10] using the satellite orbital information. Then spectra were unfolded using a Bayesian unfolding procedure [11] in order to take into account energy losses in the instrument and the tracker resolution on the rigidity reconstruction. In this way the energy spectra at the top of the payload were obtained. After the unfolding procedure the spectra were combined accounting for the proper live times and acceptance using only the fluxes at energies that exceeded 1.3 times the maximum vertical geomagnetic cutoff at each cutoff interval, thus excluding contamination from re-entrant albedo particles.

Figure 5 shows the electron energy spectra for 2007 and 2009 (top panel) and the ratio between the two sets of fluxes (lower panel) clearly showing the time dependence of the fluxes. It follows from this ratio that the low-energy electron flux increased by a factor of about 1.5 from 2007 to 2009. Protons at these energies, on the other hand, increased by a factor of about 2.5 over this period [6], indicating the effect of particle drifts.

5. Conclusions

We have presented new results on the electron energy spectrum obtained by the PAMELA experiment during the past extra-ordinary solar minimum period that ended in late 2009 - beginning of 2010. An analysis for low energies electrons (down to 70 MeV) as well as a more detailed study of the time dependence of the electron spectrum and its systematic uncertainties in progress and will be the topic for a future publication.

Acknowledgments

We acknowledge support from The Italian Space Agency (ASI), Deutsches Zentrum für Luft- und Raumfahrt (DLR), The Swedish National Space Board, The Swedish Research Council, The Russian Space Agency (Roscosmos) and The Russian Science Foundation. M Potgieter and E. Vos acknowledge the partial financial support from the South African Research Foundation (NRF) under the SA-Italy Bilateral Programme.

References

[1] M. S. Potgieter 2014 *Adv. Space Res.* **53** 1415-1425
[2] D. Heberm, M. S. Potgieter, 2006 *Space Science Reviews.* **127** 117
[3] P. Evenson, J. Clem, 2011 *Proc. of the 32rd Int. Cosmic Ray Conf.* (Beijing. China) **11** 52
[4] M. S. Potgieter et al. 2013 *Proc. of the 33rd Int. Cosmic Ray Conf.* (Rio de Janeiro. Brazil) arXiv:1308.1617 [astro-ph.SR]
[5] P. Picozza, et al. 2007 *Astropart. Phys.* **27** 296
[6] O. Adriani, et al. 2013 *Astrophys. J.* **765** 91
[7] O. Adriani, et al. 2009 *Phys. Rev. Lett.* **102** 051101
[8] S. Agostinelli et al. 2003 *Nucl. Instrum. Meth. A* **506** 250
[9] O. Adriani, et al. 2009 *Nature* **458** 607-609
[10] M. A. Shea, D. F. Smart, and L. Gentile 1987 *Physics of the Earth and Planetary Interiors* **48** 200
[11] G. D'Agostini 1995 *NIM* **A362** 487-498